AerospaceEurope Conference2020
BORDEAUX, FRANCE | 25 - 28 FEBRUARY 2020
HOSTED BY : 3AF

PREPARATION OF LOADS AND AEROELASTIC ANALYSES OF A HIGH ALTITUDE, LONG ENDURANCE, SOLAR ELECTRIC AIRCRAFT

Arne Voß[(1)], Vega Handojo[(1)], Christian Weiser[(2)], Steffen Niemann[(3)]

[(1)] DLR - German Aerospace Center, Institute of Aeroelasticity
Bunsenstraße 10, 37081 Göttingen, Germany
arne.voss@dlr.de, vega.handojo@dlr.de

[(2)] DLR - German Aerospace Center, Institute of System Dynamics and Control
Münchener Straße 20, 82234 Weßling, Germany
christian.weiser@dlr.de

[(3)] DLR - German Aerospace Center, Institute of Composite Structures and Adaptive Systems
Lilienthalplatz 7, 38108 Braunschweig, Germany
steffen.niemann@dlr.de

KEYWORDS

High altitude platform, HALE, Maneuver loads, gust loads, aeroelasticity, structural dynamics

ABSTRACT

High altitude, long endurance aircraft can serve as platform for scientists to make observations of the earth over a long period of time. Staying airborne only by solar electric energy is, as of today, a challenge for the aircraft design and requires an extremely light weight structure at the edge of the physically possible. This paper focuses on the loads and aeroelastic aspects of such a configuration, discusses the selected strategies and presents the applied methods and tools, including the resulting models prepared for the HAPomega configuration currently under development at the DLR. Because of the structural flexibility and the slow speed of the aircraft, flight mechanical and flight control aspects interact with aeroelastics e.g. during a gust encounter, making a non-linear time domain simulation necessary. Both maneuver and gust loads are used for the structural sizing and result in a very light and slender airframe with very low eigenfrequencies.

Figure 1: Artist impression of the HAPomega high altitude platform

1. MOTIVATION AND INTRODUCTION

The HAPomega configuration is a very light weight, high altitude and long endurance aircraft (HALE) with the mission to stay airborne and hold position for several days. Carrying optical measurement equipment, this allows scientists to make observations of the earth continuously for a long period of time. This is an advantage compared to satellites, which typically pass the same spot only every couple of days and fly much higher, leading e.g. to a lower optical resolution. In addition, purchase and operation costs of an aircraft are expected to be much lower compared to a satellite. An illustration of the HAPomega configuration, currently under development at the DLR, is shown in Figure 1.

Similar configurations, which are currently under development in the industry, are the Airbus Zephyr [2,31] (formerly developed by QinetiQ) or the Phasa-35 [38] by BAE Systems. Other comparable aircraft with and without a tail are the Solar Impuls [39] or the NASA Helios prototype [10]. The first two examples are planned for commercial use while the latter have a more scientific background. The HAPomega will hopefully unite the best of both worlds.

The aeroelastic behavior and modeling of HALE configurations is well-studied and briefly presented in the following. One important key event is probably the Helios mishap [21,22] in 2003, which got much public attention and has inspired people to start investigations. In this way the mishap had a very positive effect and shows the need to include detailed and sophisticated methods as early as possible in the design process of an aircraft. HALE configurations feature wings of a very large aspect

ratio at a very low structural weight. Thus, their wings are very flexible, can experience large deformations during flight and have low natural frequencies, possibly leading to an interaction with the aircraft's rigid body motion. In addition, structural and geometrical non-linearities should be accounted for if the deformations are very large. Both effects have been studied by many authors, e.g. Patil et al. [25–28]. Raghavan [32] concentrated on the flight dynamical part only with a rigid structure. Su and Cesnik [40] added a spatially distributed, three dimensional gust. In another work, Su and Cesnik [41] studied the phenomena of body-freedom flutter for a very flexible configuration. Naser et al. [23] wrote a comprehensive report on the Alliance 1 Proof-of-Concept Airplane under gust loads with special focus on a spanwise variation of gust velocities. The aircraft is highly flexible and has an empennage. Analyses are conducted using MSC.Nastran. Dong [6] investigated a gust encounter of a HALE using CFD, coupled with a modal (thus linear) structural representation of the aircraft. Wang et al. [46] tried to capture stall areas at the wing tip. Ricciardi et al. [33–35] evaluated the applicability of a quasi-static gust analysis using Pratt's Formula. Kotikalpudi [18] performed body freedom flutter analyses using unsteady panel aerodynamics in the time domain and made the analysis code publicly available [17] to create a common platform for research. Leitner et al. [20] investigated both body freedom flutter and gust response, comparing linear and non-linear structural modeling. Ouellette [24] compared simulation results with flight test data of the X-56A MUTT. Benassi and Aquilini [2] give insight into the structural dynamics of the Airbus Zephyr, unfortunately without giving exact values as they are confidential.

This paper will focus on the path that leads to a sophisticated loads and aeroelastic analysis. The authors will share their thoughts on the anticipated aeroelastic effects and discuss which physical aspects are considered to be important for a successful analysis. This leads to the selection of appropriate aeroelastic models, methods and tools. The resulting aeroelastic models prepared for the current preliminary design are presented. Because the aeroelastic behavior is an important part of the aircraft design, the interaction with other disciplines is discussed and the selected approaches are shown, such as for the structural design and the interaction with the flight control system. This paper can be considered as the first in a series of planned publications: whether the selected strategy is successful or needs improvement, will be shown in future papers, including possible failures and results.

a) 2-Dimensional profiles and locations

b) 3-Dimensional geometry

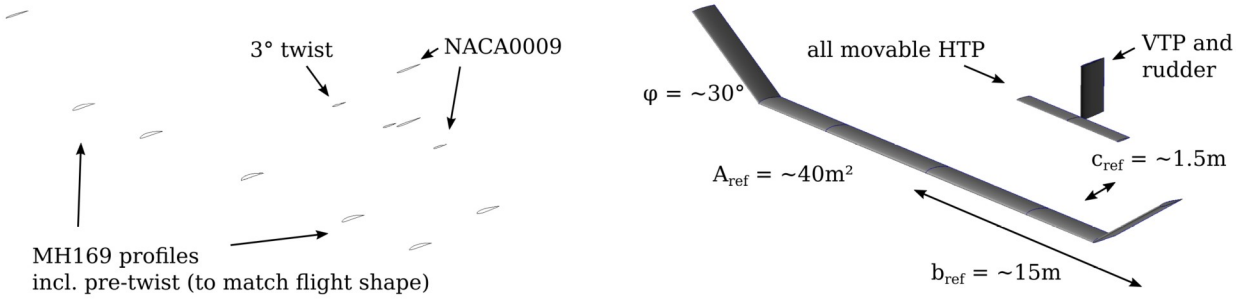

c) Geometric layout, meshed with finite elements

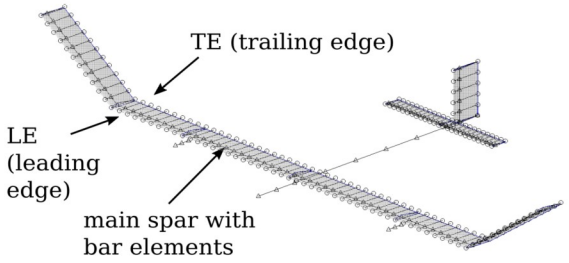

Figure 2: From basic planform to FE model

2. THE HAPomega CONFIGURATION

The idea is to create a flight vehicle that flies very slow but is highly efficient and powered by solar electric energy. This requires a design which offers large areas for the installation of solar panels and is very light weight at the same time. During the night, the altitude is decreased and batteries are used, which are then re-charged during daytime. The comparatively large winglets are motivated by the aim to capture more sunlight in the morning and evening. For exploring the parameter space and for finding a configuration that is feasible form an energetic point of view, a design framework was used, which is formally described in [36,37]. Basic loads and flight physical assumptions were incorporated to estimate e.g. the structural weight or the control surface sizes. Based on those analyses, the proposed configuration parameters are selected such that they fulfill the design missions as described in [14] at different times of the year (summer, winter) and locations on the earth. The planform as well as the main parameters are shown in Figure 2. The aircraft has a design weight of 135 kg at a wing span of ~30 m and a projected area of ~40 m², which leads to a very low wing loading of < 4.0 kg/m². The rectangular wing is selected as it offers maximum space for the solar generators, which are typically manufactured as rectangular panels. The empennage has a conventional layout, but the horizontal tailplane is planned as an all movable control surface. This has the advantage that if the hinge line is located at 25%, the attachment is nearly free from any moments and allows for a smaller and lighter actuation system. To save weight, there will be no ailerons and rolling is achieved by yawing the aircraft in combination with the V-shape of the winglets. When the aircraft needs to start and land repeatedly e.g. during flight test, small low speed ailerons are thinkable, which are deactivated when not needed. The fuselage is a simple beam construction connecting wing and empennage and carries an aerodynamically shaped housing for the payload of up to 5 kg as well as for avionic and communication systems. Two engines will be installed at ±6.0 m in span-wise direction.

The designed maneuvering speed is 9.1 m/s EAS with a stall speed at 6.5 m/s EAS and a maximum cruise speed of 12.4 m/s EAS. The altitude ranges from sea level up to 24.0 km, as the aircraft is supposed to fly most of the time above the regular air traffic, except for climb and descent phases. The airfoils of the wing (MH169 airfoil family) are specially designed to deliver optimal performance under these operational conditions. The aerodynamic design also includes a desired lift distribution of the wing in its flight shape, which can be achieved by including a pre-twist of the profiles along the wing during manufacturing.

Note that the presented configuration is a preliminary design (version HAP-O2), which will be subject to change as the project progresses and the design becomes more detailed. From an aeroelastic perspective, the proposed design is accepted as a given. The authors believe that the proposed design is feasible from an overall point of view, so that general changes to the configuration are not expected and the presented work is representative.

Next to the flight physical aspect, there are several other important topics that need to be considered. Key elements, not discussed in this paper, are high performance solar generators and batteries that also operate at high temperature differences between day and night. Therefor, disciplines such as thermal management of the electronic components as well as of the payload are very important. Other topics that need consideration include communication, data transfer or the integration into airspace.

3. LOADS AND AEROELASTIC CONSIDERATIONS AND MODELING

Typically, the smaller the aircraft (and the less damage in case of failure), the more simple the applied numerical methods. In addition, small manufacturers simply don't have the capacity for very detailed numerical analyses. This may be a reasonable approach, but leads to high safety margins, additional safety equipment such as parachutes and, presumably, a heavy and over-sized design. Clearly, this is not an option for the HAPomega configuration.

In general, the methods selected for this work are derived from the methods used in the design of large transport aircraft certified by CS-23 [9] or CS-25 [8]. The authors believe that the level of detail that comes with these methods is necessary to capture the aeroelastic behavior of the HAPomega configuration adequately. Only the level of detail, the reliability and the trust into the numerical analyses enables the extreme light weight design. Still, these methods are applied at

a) the edge of the physically possible and

b) the edge of the region of their validity.

3.1. Structural Modeling

The wing structure consists of one main spar plus 34 ribs, located at evenly spaced intervals along the wing. The main spar is a tube made from carbon fiber reinforced plastics and the fibers will be wound about a cone to create the tube. The

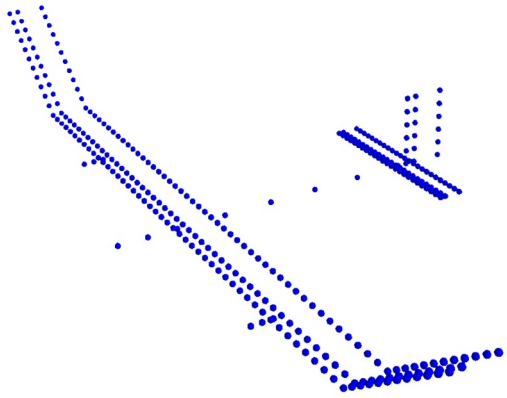

Figure 3: Structural discretization of the HAP-O2 configuration

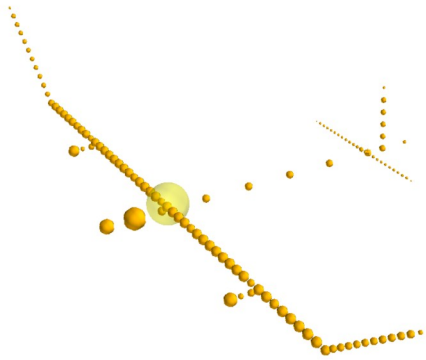

Figure 4: Mass modeling of the HAP-O2 configuration

tube will be of variable diameter and variable material thickness. The sizing of the tube will be discussed in section 5.1. The wing will be covered with a foil-type skin with the solar generators just below the skin or glued on top.

Therefor, the aeroelastic modeling of the structure uses a finite elements model with beams elements as well, shown in Figures 2 c) and 3, which represent the long and slender structure adequately and are very close to the actual structural design. The beam model is discretized at every rib station along the wing and comprises a leading and trailing edge connected with rigid body links to the main spar. The main purpose is to visualize effects such as the wing torsion.

The authors suspect that the aircraft is more likely to have a stiffness problem than a structural strength problem. Therefor, the main spar is located at 25 % in chord direction, which is slightly in front of the maximum airfoil thickness. However, this is a favorable location when thinking of divergence and creates little or no additional elastic torsion e.g. during a gust encounter, which leads to lower structural loads.

A modal analysis in combination with a modal truncation is performed on the mass and stiffness matrices $\mathbf{M}_{gg}$ and $\mathbf{K}_{gg}$, which are are extracted from MSC.Nastran. The modes are selected up to a frequency of 20 Hz and in such a way that at least the first bending and torsional modes of every component are included, which currently leads to 32 modes. Note that the selected structural modeling and the modal approach are limited to the linear elastic region only. First studies have shown a wing tip deflection in the region of 10% of the half wing span and the assumption of linearity is still considered as acceptable.

3.2. Mass Modeling

Structural masses are derived from the material thickness and material density. The non-structural masses of the wing include the solar generators, the battery packs and the engines. Because the torsional eigenmodes and -frequencies of the wing are very sensitive, special attention needs to be put on the inertia properties about y-axis and the location of the masses in x-direction.

Both mass and inertia properties are then modeled as condensed masses, which are attached to the structural grid points of the finite elements model. A visualization is shown in Figure 4, where each sphere represents the masses attached to one grid point and the large, transparent yellow sphere visualizes the center of gravity of the aircraft.

Because there are no fuel tanks and the payload has a fixed location in the aircraft nose, currently only one design mass case is required.

3.3. Aerodynamic Modeling

Although the aircraft flies very slowly at sea level, the true airspeed at high altitudes leads to surprisingly high speeds with Mach numbers up to 0.3. Still, the flight speed is fully within the subsonic regime and panel methods such as the steady vortex lattice method (VLM) and the unsteady doublet lattice method (DLM) yield an acceptable representation of the lifting surfaces. The formulation of the VLM used herein follows closely the derivation given by Katz and Plotkin [16] using horse shoe vortices. The DLM is formulated as presented by Albano and Rodden [1]. Compressibility (in the subsonic regime) is accounted for by the Prandtl-Glauert transformation with $\beta = \sqrt{(1 - Ma^2)}$, which is applied to the VLM as suggested by Hedman [12]. Both methods require the geometry as input, discretized with aerodynamic panels shown in

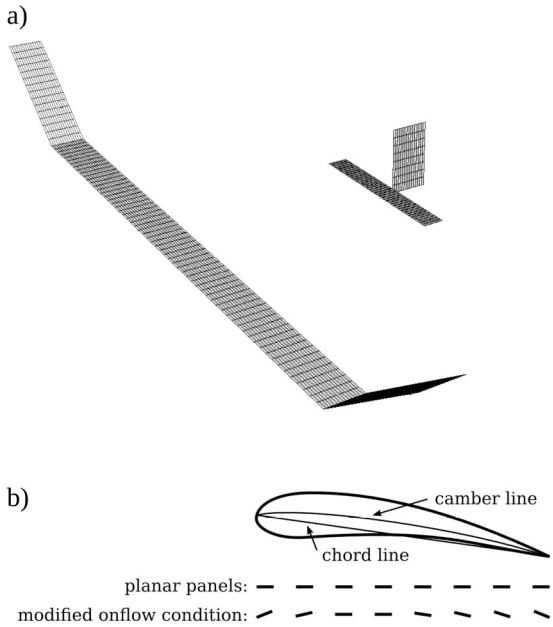

Figure 5: Discretization of the lifting surfaces with an aerodynamic panel mesh and correction of camber and twist

Figure 5. It can be seen that the lifting surfaces are modeled as a flat plate, but camber of the airfoils and the twist of the wing can be included by a modification of the onflow condition, as sketched in Figure 5 b). Matrices of aerodynamic influence coefficients $\mathbf{AIC}(Ma, k)$ are calculated depending on the Mach number and the reduced frequency. The extremely slow flight at sea level leads to very high reduced frequencies k defined by

$$k = \frac{c_{ref}}{2V} \cdot \omega \,, \tag{3.1}$$

which require a good discretization with at least 16 panels in chord direction.

3.4. Aero-Structural Coupling

In a next step, the aerodynamic forces need to be applied to the structure. Formally, the coupling can be handled using a transformation matrix $\mathbf{T}_{kf}$ which relates displacements of the structural grid $\mathbf{u}_f$ to displacements of the aerodynamic grid $\mathbf{u}_k$ with

$$\mathbf{u}_k = \mathbf{T}_{kf} \cdot \mathbf{u}_f. \tag{3.2}$$

In addition, the transposed matrix $\mathbf{T}_{kf}^T$ transfers forces and moments from the aerodynamic grid $\mathbf{p}_k$ to the structural grid $\mathbf{p}_f$ with

$$\mathbf{p}_f = \mathbf{T}_{kf}^T \cdot \mathbf{p}_k. \tag{3.3}$$

Note that the structural displacements and loads (index 'f') are not given in physical but in modal coordinates, as mentioned in section 3.1. The size of the problem depends on the degrees of freedom

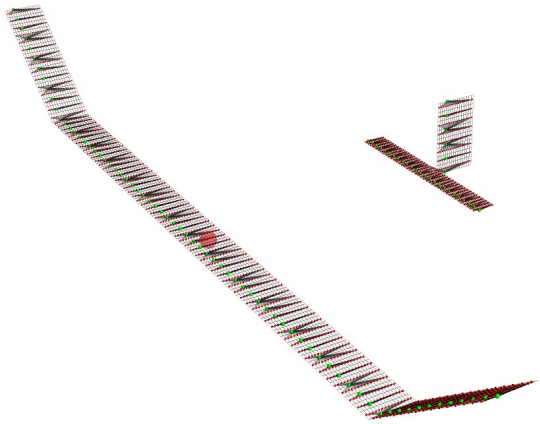

Figure 6: Structural discretization of the HAP-O2 configuration

of both the aerodynamic and structural grid. In this case, the structural grid has 1932 degrees of freedom. Therefore, a projection into modal coordinates in combination with a truncation of higher frequency modes implies a significant reduction.

In general, a transformation matrix $\mathbf{T}_{di}$ may be defined by various methods [45]. One approach for loads calculation is the rigid body spline. Each grid point of the dependent grid is mapped to exactly one point on the independent grid. The distance $\mathbf{d} = [d_x, d_y, d_z]^T$ between these two grid points is assumed as a rigid body that transfers forces and moments. In addition, forces $\mathbf{f}$ create moments $\mathbf{m}$ due to their lever arm

$$\mathbf{m} = \mathbf{d} \times \mathbf{f}. \tag{3.4}$$

In reverse, translations and rotations are directly transferred and rotations create additional translations. The rigid body spline is suitable for aerodynamic panel methods and avoids large nonphysical, local nodal forces that may occur with other methods such as a surface or volume spline. This is an important aspect when calculating nodal and/or section loads for the structural sizing.

3.5. Flight Mechanical Interaction

Because of the slow flight and the low wing loading, first simulations showed a strong flight mechanical reaction e.g. during a gust encounter. For loads analyses, this has several consequences.

First, the interaction with flight mechanics needs to be included in the loads analyses. The motion of the aircraft is divided into a rigid and a flexible part. For the rigid body motion, the aircraft is considered as a point mass with inertia matrices $\mathbf{M}_b$ and $\mathbf{I}_b$, where the components of the inertia tensor $\mathbf{I}_b$ are calculated with respect to the body axes 'b'. Its

origin is positioned at the center of gravity. All external forces and moments $\mathbf{p}_g^{ext}$ are gathered at the same point. The non-linear equations of motion given by

$$\dot{\mathbf{v}}_b = \mathbf{M}_b^{-1} \cdot \mathbf{p}_b^{\text{ext, forces}} + \mathbf{v}_b \times \boldsymbol{\omega}_b + \dot{\mathbf{v}}_b^{\text{grav}} \tag{3.5}$$

and

$$\dot{\boldsymbol{\omega}}_b = \mathbf{I}_b^{-1} \cdot \left(\mathbf{p}_b^{\text{ext, moments}} - \boldsymbol{\omega}_b \times (\mathbf{I}_b \cdot \boldsymbol{\omega}_b)\right) \tag{3.6}$$

yield the translational and rotational accelerations $\dot{\boldsymbol{\omega}}_b$ and $\dot{\mathbf{v}}_b$ of the aircraft body frame. The coupling terms between translation and rotation $\mathbf{v}_b \times \boldsymbol{\omega}_b$ and $\boldsymbol{\omega}_b \times (\mathbf{I}_b \cdot \boldsymbol{\omega}_b)$ are derived by Waszak, Schmidt and Buttrill [4,47,48]. Gravitational acceleration is accounted for by $\dot{\mathbf{v}}_b^{\text{grav}}$ in equation (3.5).

In addition to the rigid body motion of the aircraft, linear structural dynamics are incorporated by

$$\mathbf{M}_{ff}\ddot{\mathbf{u}}_f + \mathbf{D}_{ff}\dot{\mathbf{u}}_f + \mathbf{K}_{ff}\mathbf{u}_f = \mathbf{p}_f^{ext} \tag{3.7}$$

Here, generalized external forces $\mathbf{p}_f^{ext}$ interact with linear elastic deflections $\mathbf{u}_f$, velocities $\dot{\mathbf{u}}_f$ and accelerations $\ddot{\mathbf{u}}_f$. The matrices $\mathbf{M}_{ff}$, $\mathbf{D}_{ff}$ and $\mathbf{K}_{ff}$ refer to the generalized mass, damping, and stiffness matrices

Second, a fully dynamic, non-linear time domain simulation is required. Typically, the gust encounter is studied in the frequency domain, as the unsteady aerodynamics are defined by the DLM in the frequency domain. However, the frequency domain is limited by its linearity and is therefore not applicable is this case. The time simulation is performed by an integration of the above equations over a period of time. Two different integration schemes have been tested. The explicit Runge-Kutta method of 4th/5th order [7] and an implicit Adams-Bashforth method [3], both implemented in Scipy [42], have shown numerically equivalent results. Because of the fewer function evaluations, the Adams-Bashforth method is selected.

Note that the flight mechanical representation is limited by the aerodynamic solution, which was selected with a focus on loads and aeroelasticity, not on flight mechanics. The vortex lattice method used herein captures for example the penetration of the aircraft into a gust and all vertical forces adequately, but does not capture drag and other coefficients that lead for example to a roll-yaw coupling. Therefore, it does not replace a full flight mechanical analysis!

3.6. Flight Control

In close connection to the flight mechanical interaction, first observation showed that the encounter of a design gust is only possible with active flight control. Although the aircraft is naturally stable, the slow flight speed in combination with the penetration of the aircraft into the gust, leads to a severe pitch-up motion with large pitch angles Θ. This quickly leads to a loss of speed and the real aircraft would stall. Therefor, a flight control system is needed that maintains the speed and the flight path of the aircraft.

From an loads and aeroelastic perspective, this means the need for closed loop gust encounter analyses already at the very beginning of the design phase.

The flight control system for the HAP omega configuration consists of an auto-pilot and flight control system (AFCS). The selected AFCS structure has been developed and validated during simulation and flight test campaigns carried out for previous high altitude platform projects [15]. The longitudinal augmentation of the AFCS has two main components: a Total Energy Control autopilot system (TECS) and an inner loop which has been newly designed for HAP omega and contains a pitch attitude control law.

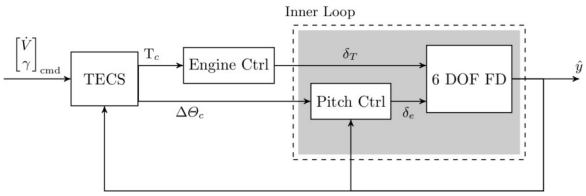

Figure 7: Proposed control architecture for longitudinal motion

The control scheme used for the longitudinal motion is presented in Figure 7. Inputs to this control law are the commanded derivative of calibrated airspeed $\dot{V}$ and the commanded flight path angle γ. TECS output commands are the thrust requirement which is directly passed to the engine. The second output is pitch attitude command which is then processed in an inner loop pitch tracker.

The TECS algorithm has been originally developed by Lambregts [19]. It decouples path variable and airspeed rate by distinguishing between mechanical energy of the aircraft and energy distribution into potential and kinetic energy. This is especially useful for the HAP application as potential energy is used as a secondary energy storage besides the batteries. The aircraft operates in a low airspeed regime close to stall speed, thus speed command will be prioritized which means that e.g. in case of a gust encounter the AFCS will ensure tracking of calibrated airspeed command while deprioritizing the flight path angle.

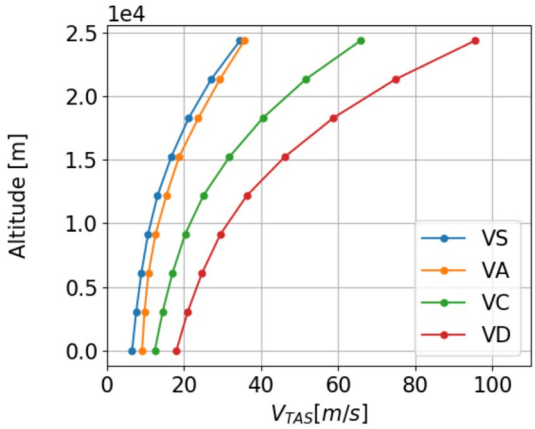

Figure 8: Proposed design speeds and altitudes

Considering outputs of the TECS autopilot, the thrust command is directly passed to the propulsion command unit. Inner loops may be necessary for stabilization at high altitude and low air density, thus are added to the control scheme. Switching the TECS algorithm off will enable Θ command. This setup was used for the gust simulations in this work, as the autopilot loop is of lower frequency and thus not interfering with pitch tracking in case of gust encounter.

The lateral axis control follows a similar layout and will be equipped with a total heading control system (THCS) which follows similar design principles as TECS. This shall ensure tracking of heading commands with zero sideslip. As control surface layout for lateral motion of HAP omega has not been finalized yet the implemented lateral control augmentation is preliminary. For gust simulation, a yaw damper and yaw angle tracker were implemented.

The control system for both longitudinal and lateral axes is in an integrated development process exported as a Functional Mockup Unit (FMU). This format is based on a textual in- / output description and an executable file which can be plugged into any simulation framework or real-time hardware (e.g. MATLAB / Simulink, Python, TargetLink).

4. DESIGN LOAD CASES

In general, loads are calculated as limit loads, which describe the loads that the aircraft must safely endure once during its service. From a material perspective, limit loads have to be within the linear elastic regime, no permanent deformations are allowed. These limit loads are complemented by ultimate loads, where individual structural components may deform or fail locally, compare CS 23.305 [9]. Ultimate loads are typically obtained by simple multiplication of limit loads by a factor of 1.5. Note that this is not a

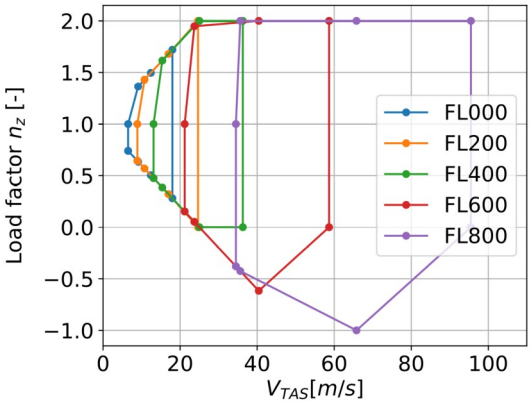

Figure 9: Maneuver flight envelope at selected flight levels

safety factor that compensates e.g. for uncertainties in the load analyses but accounts for material characteristics and for uncertainties in the material properties.

For the selection of load cases, mainly CS-23 [9] is taken as a “guideline”. Other specifications like CS-22 or CS-VLA might match better judging by the size of the aircraft but the selected methods and tools harmonize better with CS-23 or even CS-25. Note that most prescribed parameters such as load factors, speeds, etc. are too high and not directly applicable to the HAPomega configuration.

The velocities and altitudes considered for loads analysis are shown in Figure 8 and each dot marks one operation point.

4.1. Maneuver Loads

In general, the maneuver parameters (accelerations, velocities, rates, angles of attack, side slip,...) must only be as high as required for controllability and maneuverability – loads need not be calculated for situations in which the aircraft is lost anyways. However, this is a difficult task as the parameters are not clear at the beginning of the design phase when the first load estimates are required.

For vertical maneuvers, CS-23 prescribes a positive load factor of $n_{\max} = 3.8$ and a negative load factor of $n_{\min} = -1.9$. These values are not feasible for the HAPomega configuration and are reduced to $n_{\max} = 2.0$ and $n_{\min} = -1.0$. At very low flight speeds, this would still require very abrupt and sharp pull-up or push-down maneuvers with very tiny radii and very high pitch rates q, which are nonphysical because of the damping of the horizontal tail. Therefore, with

$$n_z = \frac{q \cdot V}{9.81} + 1.0 \tag{4.1}$$

and a maximal allowed pitch rate $q_{\max} = 0.2\ \mathrm{rad/s}$, the load factors n_z are limited further at low speeds. Figure 9 shows the envelope for vertical maneuvers at different operation points. Note that in areas of slow flight speed, the envelope is very small and will presumably not dimension the aircraft.

4.2. Gust Loads

As an alternative to the 1-cos gust, in some cases the Pratt formula is used, especially for smaller aircraft. Following Pratt, gusts are converted to an equivalent load factor n_z based on a mass ratio μ_g and a gust factor kg. More detailed information can be found in CS 23.341 [9] and in NACA Technical Note 2964 [29] and Report 1206 [30]. The loads are then calculated as quasi-static maneuvers for both positive and negative gusts. Handojo and Klimmek [11] found a very good agreement for a transport aircraft with forward-swept wings and Voß and Klimmek [43,44] studied the applicability of the Pratt formula on flying wings. However, application of the Pratt formula for the HAPomega configuration is questionable because the underlying database did not include very light weight vehicles, which is confirmed by Ricciardi et al. [33–35]. With $\mu_g = 0.51$, the mass ratio of HAPomega is at the border of the parameter space investigated by Pratt and Walker and their curve fit shows a high gradient in that region, leading to a high sensitivity of gust factor kg to small variations in μ_g. Therefor, 1-cos gust simulation following CS-25 are more physical.

The prescribed gust velocities of CS-25 are only given up to FL600. The data given in Hoblit [13] (see Fig. 4.16) and in MIL-HDBK-1797 [5] (see Fig. 262) shows that the gust velocities / probabilities decrease further up to FL800. Therefore, continuing the linear relationship from FL600 up to FL800 appears reasonable. In addition, a time span of 2 days at low altitudes and 100 days above FL600 is assumed. Furthermore, take-off, climb, descent and landing must take place under monitored weather conditions. These assumptions and the comparison of the gust velocities for a transport aircraft with a life span of ~50.000h suggests that the prescribed gust velocities of CS-25 may be reduced by a factor of 0.5 for the HAPomega configuration.

For the design load cases, gust from various directions are considered, as sketched in Figure 10, where 0/360° indicates an upward gust. Vertical gusts hit both the wing and horizontal tail most while lateral gusts have the largest impact on the vertical tail. Additional gusts are placed orthogonal to the winglets, which not only have an impact on the winglets themselves but might create

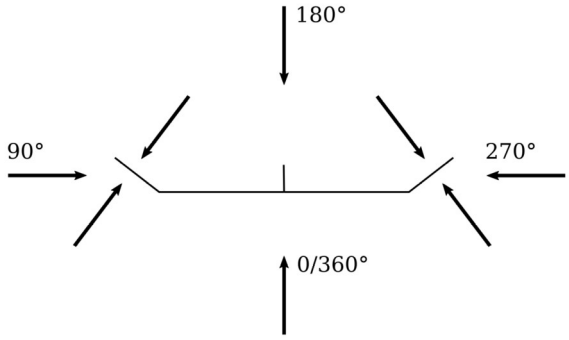

Figure 10: Schematic sketch of gust directions

high wing root bending moments due to the long lever arm. Finally, torsional moments are expected in the wing due to pitch accelerations and the out-of-plane masses of the large winglets.

Summing up, the gust loads analyses for the HAPomega configuration requires a non-linear, fully dynamic simulation in the time domain that includes the penetration of the aircraft into the gust, the flight mechanical reaction and the interaction with the flight control system. Not that typically also unsteady effects are included, but have been omitted because of problems with the approximation (RFA) that is required for the translation of the unsteady terms from the frequency into the time domain. Investigations on this topic are ongoing, but the quasi-steady approach is considered to be conservative as the unsteady aerodynamics typically decrease and add a delay to the impact of the gust.

4.3. Selection of Dimensioning Load Cases

Type	Load cases
Maneuver	378
Gust	738
Landing	7

Table 1: Overview of load cases

Next to the vertical maneuvers described in section 4.1, there are several other maneuver cases including rolling, yawing and side-slip conditions. Application of these maneuver cases to the corresponding operation points leads to a total of 378 maneuver load cases. Because gusts are calculated at five different gust gradients ranging from $H = 9.0$ to $61.0m$ (half of gust length), the number of gust load cases is even higher. The largest gust gradient is smaller compared to that defined in CS-25 with $H = 107.0$ m since these do not evoke large loads anymore - because of the low airspeeds. Finally, seven different dynamic landing cases are considered. Note that these are the numbers for just one mass configuration and

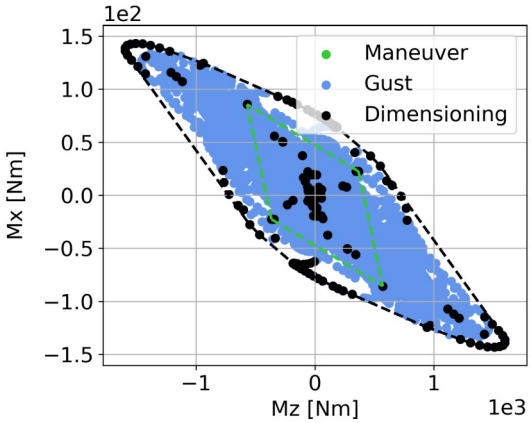

Figure 11: Identification of dimensioning load cases using load envelopes and the convex hull

the numbers scale linearly with every additional mass case.

The resulting nodal loads are integrated e.g. along the wing at so-called monitoring stations to create section loads. For the wing, interesting quantities are for example the shear force F_z, bending moment M_x or torsional moment M_y.

The dimensioning load cases are identified with two-dimensional load envelopes which show a combination of two interesting quantities / section loads. An example is shown in Figure 11. Every dot corresponds to one load case and for dynamic loads, time slices are used, allowing to merge maneuver and gust loads. In a next step, the convex hull is determined to identify the dimensioning load cases at every monitoring station. Note that because correlated section loads are used, not all dimensioning load cases lie on the convex hull of every monitoring station. In the example below, there are black dots also in the center of the envelope.

For the whole aircraft, about 100 dimensioning load cases are identified, which lead to about 240 correlated sets of section loads. This is because for example a gust or landing case may cause dimensioning loads at different components at different times. These per-selected sets of dimensioning section loads are then used for the sizing of the airframe.

5. RESULTS

5.1. Structural Sizing

The structural design of the overall aircraft is carried out with an algorithm based on analytical methods. For this purpose, a beam model of the aircraft with all main components is generated. The mass calculation is performed with this model by dimensioning the main structural elements (Bernoulli beam theory), which are the wing and tail spars and the longerons (pylons, nacelles or fuselages). The masses of other elements like ribs, wing outer skin including solar generator or joining elements are scaled volumetrically or two-dimensionally, which is considered as adequate for the current level of detail.

As main structural element, a tube spar is chosen for the wing spars and for the longerons (fuselage, engine nacelle). The reasons for this are the very low wing loading (resulting in very thin laminate thicknesses), manufacturing aspects (winding technology vs. costs for shell tools) and assembly considerations (joining the individual parts to form a complete wing spar, positioning the ribs, etc.).

The sizing criteria of the beam elements are material strength, stability and demands on torsional and bending stiffness. The dimensioning parameters are the tube thickness, tube diameter, the rib or frame distance and material parameters (laminate stacking). As material model, a smeared winding laminate is considered, so that the thickness is the only design parameter, while different laminates with smeared stiffness and strength properties are pre-selected. Application of a minimum material thickness prevents non-producable designs.

Because the structural masses and properties influence the loads and vice versa, the sizing process is realized as an iterative procedure:

Step 1: An initial structural design is created based on two initial load cases

Step 2: Comprehensive loads analysis and pre-selection of dimensioning load cases based on the initial design

Step 3: Structural sizing based section loads from the comprehensive loads analysis

Step 4: Update of the aeroelastic model

After the first initial step, steps 2 to 4 are repeated until a mass convergence is achieved. Note that even though a pre-selection of the dimensioning load cases is performed, a large number of load cases still needs to be processed during the sizing in step 3. Therefor, the aircraft is sized once for every set of correlated section loads and the biggest material thicknesses of each section yield the new thickness distribution. Finally, this design is cross-checked against all load cases.

In the case of the HAPomega configuration, convergence is achieved after three iterations, resulting in a mass breakdown as given in Table 2.

Component	Mass [%]
Wing	27%
Longeron	8%
Tail	2%
Systems	6%
Devices	6%
Payload	4%
Batteries	47%
Platform	100%

Table 2: Overview of resulting mass breakdown after structural sizing

5.2. Structural Dynamic Characteristics

The eigenforms and -frequencies characterize the structural dynamic behavior of an aircraft and are important for further aeroelastic analyses. A summary of the first eigenmodes is given in Table 3. As expected, the long and slender wings show very low eigenfrequencies. The first symmetric wing bending, visualized in Figure 12, has a frequency of only 0.80 Hz. Because the tube-type spar has the same stiffness properties in all directions, the first in-plane wing bending (0.81 Hz) is very close to the first wing bending. The eigenmodes 5 (see Figure 13) and 6 show the first symmetric and asymmetric wing torsion with 1.89 Hz and 2.22 Hz respectively. This is also very low and can be explained by the low torsional stiffness of the main spar and by the out-of-plane masses of the large winglets. It can be concluded that for example ailerons would have a low effectiveness from an aeroelastic perspective and should be located at the inner part of the wing. Also, the first fuselage bending mode (Table 3, mode 10) has a rather low frequency with 4.73 Hz, which presumably reduces the control surface efficiency of the tail, too.

6. SUMMARY AND FUTURE WORK

In this paper, the strategies for the aeroelastic modeling of the HAPomega configuration are presented. The authors believe that the level of detail of the selected methods and models is required for a sophisticated analysis of such an extremely light weight configuration. The interaction with other disciplines such as flight mechanics, flight control and structural sizing is discussed. The aeroelastic models can be seen as a result of the structural sizing procedure and are a result of this paper. First insights on the structural dynamics characteristics were shown and revealed a very flexible structure with low eigenfrequencies. A more detailed analysis of the dimensioning load cases is planned for the next paper.

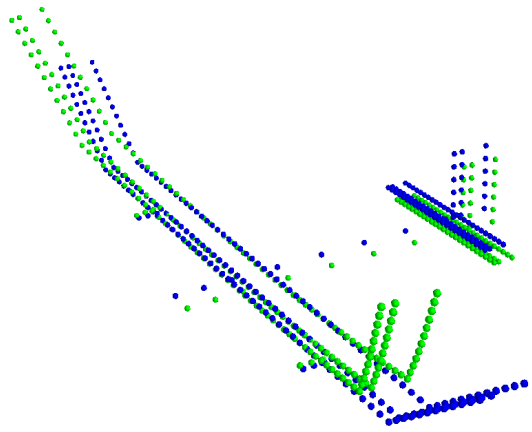

Figure 12: Mode 1, first symmetric wing bending

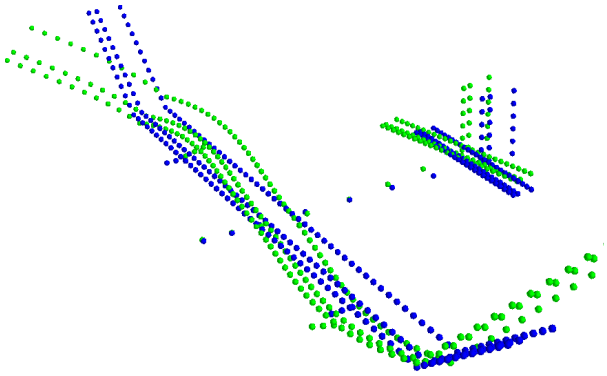

Figure 13: Mode 5, first asymmetric wing torsion

#	Description	Frequency
1	1st wing bending, symmetric	0.80 Hz
2	1st in-plane wing bending, symmetric	0.81 Hz
3	1st in-plane wing bending, asymmetric	1.16 Hz
4	1st wing bending, asymmetric	1.81 Hz
5	1st wing torsion, asymmetric	1.89 Hz
6	1st wing torsion, symmetric	2.22 Hz
7	2nd wing bending, symmetric	2.69 Hz
8	2nd in-plane wing bending, asymmetric	3.96 Hz
9	2nd wing bending, symmetric	4.41 Hz
10	1st fuselage bending	4.73 Hz

Table 3: Overview of the first eigenforms and -frequencies

Future work includes the analysis of the jig and flight shape, which determines the pre-twist of the airfoils along the wing. Control surface effectiveness due to aeroelastic deformation needs to be determined and a flutter check needs to be performed. Flight control system modes for the different flight phases (e.g. landing, ascent / descent, ...) need to be developed and tested thoroughly. A study that considers geometrical and structural non-linearities could be performed to check if the assumption of linearity holds true and to quantify any differences. For the final aircraft, different tests are planned, including a ground vibration test to identify the structural dynamic properties experimentally. This will be the basis for an update of the simulation models and for a comprehensive flutter analysis.

REFERENCES

[1] Albano, E., and Rodden, W. P., “A Doublet Lattice Method For Calculating Lift Distributions on Oscillation Surfaces in Subsonic Flows,” in *AIAA 6th Aerospace Sciences Meeting*, New York, 1968.

[2] Benassi, L., and Aquilini, C., “The Structural Dynamics of Flying Non Stop for 100 Days,” presented at the 18th International Forum on Aeroelasticity and Structural Dynamics, Savannah, Georgia, 2019.

[3] Brown, P. N., Byrne, G. D., and Hindmarsh, A. C., “VODE: A Variable-Coefficient ODE Solver,” *SIAM Journal on Scientific and Statistical Computing*, vol. 10, no. 5, pp. 1038–1051, Sep. 1989, https://doi.org/10.1137/0910062.

[4] Buttrill, C., Zeiler, T., and Arbuckle, P., “Nonlinear simulation of a flexible aircraft in maneuvering flight,” in *Flight Simulation Technologies Conference, Guidance, Navigation, and Control and Co-located Conferences*, 1987, https://doi.org/10.2514/6.1987-2501.

[5] Department of Defense, ed., *MIL-HDBK-1797 FLYING QUALITIES OF PILOTED AIRCRAFT*. 1997.

[6] Dong Guo, Xu, M., and Shilu Chen, “Nonlinear Gust Response Analysis of Free Flexible Aircraft,” *International Journal of Intelligent Systems and Applications*, vol. 5, no. 2, pp. 1–15, Jan. 2013, https://doi.org/10.5815/ijisa.2013.02.01.

[7] Dormand, J. R., and Prince, P. J., “A family of embedded Runge-Kutta formulae,” *Journal of Computational and Applied Mathematics*, vol. 6, no. 1, pp. 19–26, Mar. 1980, https://doi.org/10.1016/0771-050X(80)90013-3.

[8] European Aviation Safety Agency, ed., *Certification Specifications for Large Aeroplanes CS-25*, Amendment 16. 2015.

[9] European Aviation Safety Agency, ed., *Certification Specifications for Normal, Utility, Aerobatic, and Commuter Category Aeroplanes CS-23*, Amendment 3. 2012.

[10] Gibbs, Y., “NASA Armstrong Fact Sheet: Helios Prototype,” *NASA*, 13-Aug-2015. [Online]. Available: http://www.nasa.gov/centers/armstrong/news/FactSheets/FS-068-DFRC.html. [Accessed: 24-Mar-2017].

[11] Handojo, V., and Klimmek, T., “Böenlastanalyse der vorwärts gepfeilten ALLEGRA-Konfiguration,” in *Deutscher Luft- und Raumfahrtkongress*, Rostock, 2015.

[12] Hedman, S. G., “Vortex Lattice Method for Calculation of Quasi Steady State Loadings on Thin Elastic Wings in Subsonic Flow,” FFA Flygtekniska Försöksanstalten, Stockholm, Sweden, FFA Report 105, 1966.

[13] Hoblit, F. M., *Gust Loads on Aircraft: Concepts and Applications*. Washington DC: American Institute of Aeronautics and Astronautics, 1988, http://arc.aiaa.org/doi/book/10.2514/4.861888.

[14] Kaltenhäuser, S., and Nikodem, F., “Operation and operation approval of high altitude platforms (HAP),” presented at the Deutscher Luft- und Raumfahrtkongress 2019, Darmstadt, 2019, https://elib.dlr.de/131061/.

[15] Kastner, N., and Looye, G., “Generic tecs based autopilot for an electric high altitude solar powered aircraft,” presented at the EuroGNC 2013, 2nd CEAS Specialist Conference on Guidance, Navigation & Control, Delft, The Netherlands, 2013.

[16] Katz, J., and Plotkin, A., *Low-speed aerodynamics: from wing theory to panel methods*. New York: McGraw-Hill, 1991.

[17] Kotikalpudi, A., “Body Freedom Flutter (BFF) Doublet Lattice Method (DLM),” *University of Minnesota Digital Conservancy*, 09-Sep-2014. [Online]. Available: http://hdl.handle.net/11299/165566. [Accessed: 12-Feb-2016].

[18] Kotikalpudi, A., Pfifer, H., and Balas, G. J., “Unsteady Aerodynamics Modeling for a Flexible Unmanned Air Vehicle,” in *AIAA Atmospheric Flight Mechanics Conference*, Dallas, Texas, 2015, https://doi.org/10.2514/6.2015-2854.

[19] Lambregts, A. A., “TECS Generalized Airplane Control System Design – An Update,” in *Advances in Aerospace Guidance, Navigation and Control*, Berlin, Heidelberg, 2013, pp. 503–534, https://doi.org/10.1007/978-3-642-38253-6_30.

[20] Leitner, M., Knoblach, A., Kier, T. M., Moreno, C. P., Kotikalpudi, A., Pfifer, H., and Balas, G. J., “Flight Dynamics Modeling of a Body Freedom Flutter Vehicle for Multidisciplinary Analy-

ses," 2015, https://doi.org/10.2514/6.2015-0905.

[21] NASA, "Helios Mishap Photo Previews," *NASA News*. [Online]. Available: https://www.nasa.gov/centers/dryden/news/ResearchUpdate/Helios/Previews/index.html. [Accessed: 05-Mar-2018].

[22] NASA, "NASA Releases Helios Prototype Aircraft Mishap Report," *NASA News*, 27-Nov-2004. [Online]. Available: http://www.nasa.gov/centers/dryden/news/NewsReleases/2004/04-42.html. [Accessed: 05-Mar-2018].

[23] Naser, A. S., Pototzky, A. S., and Spain, C. V., "Response of the Alliance 1 Proof-of-Concept Airplane Under Gust Loads," Lockheed Martin Engineering and Sciences Company, Hampton, Virginia, Technical Report NASA CR-2001-210649, Mar. 2001, http://ntrs.nasa.gov/search.jsp?R=20010038652.

[24] Ouellette, J., "Aeroservoelastic Modeling of Body Freedom Flutter for Control System Design," presented at the 58th AIAA/ASCE/AHS/ASC Structures, Structural Dynamics, and Materials Conference, Grapevine, Texas, 2017.

[25] Patil, M., Hodges, D., and Cesnik, C., "Nonlinear aeroelasticity and flight dynamics of High-Altitude Long-Endurance aircraft," in *40th Structures, Structural Dynamics, and Materials Conference and Exhibit*, 1999, http://arc.aiaa.org/doi/abs/10.2514/6.1999-1470.

[26] Patil, M. J., and Hodges, D. H., "On the importance of aerodynamic and structural geometrical nonlinearities in aeroelastic behavior of high-aspect-ratio wings," *Journal of Fluids and Structures*, vol. 19, no. 7, pp. 905–915, Aug. 2004, https://doi.org/10.1016/j.jfluidstructs.2004.04.012.

[27] Patil, M. J., Hodges, D. H., and Cesnik, C. E. S., "Nonlinear Aeroelasticity and Flight Dynamics of High-Altitude Long-Endurance Aircraft," *Journal of Aircraft*, vol. 38, no. 1, pp. 88–94, 2001, https://doi.org/10.2514/2.2738.

[28] Patil, M., and Taylor, D., "Gust Response of Highly Flexible Aircraft," presented at the 47th AIAA/ASME/ASCE/AHS/ASC Structures, Structural Dynamics, and Materials Conference, Newport, Rhode Island, 2006, http://arc.aiaa.org/doi/abs/10.2514/6.2006-1638.

[29] Pratt, K. G., "A revised formula for the calculation of gust loads," National Advisory Committee for Aeronautics. Langley Aeronautical Lab., Langley Field, VA, Technical Note TN 2964, Jun. 1953, http://ntrs.nasa.gov/search.jsp?R=19930084025.

[30] Pratt, K. G., and Walker, W. G., "A Revised Gust-Load Formula and a Re-evaluation of V-G Data Taken on Civil Transport Airplanes From 1933 to 1950," National Advisory Committee for Aeronautics. Langley Aeronautical Lab., Langley Field, VA, Technical Report NACA-TR-1206, 1953.

[31] QinetiQ Group plc, "QinetiQ's Zephyr UAV exceeds official world record for longest duration unmanned flight," *QinetiQ*, 10-Sep-2007. [Online]. Available: https://www.qinetiq.com/media/news/releases/Pages/qinetiqs-zephyr-exceeds-world-record.aspx. [Accessed: 24-Mar-2017].

[32] Raghavan, B., and Patil, M., "Flight Dynamics of High Aspect-Ratio Flying Wings," in *AIAA Atmospheric Flight Mechanics Conference and Exhibit*, American Institute of Aeronautics and Astronautics.

[33] Ricciardi, A., "Utility of Quasi-Static Gust Loads Certification Methods for Novel Configurations," Master Thesis, Virginia Polytechnic Institute and State University, Blacksburg, Virginia, 2011.

[34] Ricciardi, A. P., Patil, M. J., Canfield, R. A., and Lindsley, N., "Evaluation of Quasi-Static Gust Loads Certification Methods for High-Altitude Long-Endurance Aircraft," *Journal of Aircraft*, vol. 50, no. 2, pp. 457–468, Mar. 2013, https://doi.org/10.2514/1.C031872.

[35] Ricciardi, A., Patil, M., Canfield, R., and Lindsley, N., "Utility of Quasi-Static Gust Loads Certification Methods for Novel Configurations," presented at the 52nd AIAA/ASME/ASCE/AHS/ASC Structures, Structural Dynamics and Materials Conference, Denver, Colorado, 2011, http://arc.aiaa.org/doi/abs/10.2514/6.2011-2043.

[36] Schumann, H., Berres, A., Escher, S., and Stehr, T., "PARADIGMshift: A Method for Feasibility Studies of New Systems," *Procedia Computer Science*, vol. 44, pp. 578–587, 2015, https://doi.org/10.1016/j.procs.2015.03.023.

[37] Schumann, H., Berres, A., Escher, S., Stehr, T., and Fricke, S., "THE PARADISE FOR PRE-DESIGNING AIRCRAFT AND SYSTEMS," presented at the Deutscher Luft- und Raumfahrtkongress (DLRK) 2013, Stuttgart, 2013, https://elib.dlr.de/85262/.

[38] Schwarz, K., "Hochfliegendes UAV: BAE übernimmt PHASA-35-Entwicklung," 10-Sep-2019. [Online]. Available: https://www.flugrevue.de/militaer/hochfliegendes-uav-bae-uebernimmt-phasa-35-entwicklung/. [Accessed: 15-Nov-2019].

[39] Solar Impulse SA, "Solar Impulse - Around the world to promote clean technologies," *Solar Impulse*. [Online]. Available: http://www.solarimpulse.com/. [Accessed: 24-Mar-2017].

[40] Su, W., and Cesnik, C., "Dynamic Response of Highly Flexible Flying Wings," presented at

the 47th AIAA/ASME/ASCE/AHS/ASC Structures, Structural Dynamics, and Materials Confere, Newport, Rhode Island, 2006, https://doi.org/10.2514/6.2006-1636.

[41] Su, W., and Cesnik, C., “Nonlinear Aeroelasticity of a Very Flexible Blended-Wing-Body Aircraft,” presented at the 50th AIAA/ASME/ASCE/AHS/ASC Structures, Structural Dynamics, and Materials Conference, Palm Springs, California, 2009, https://doi.org/10.2514/6.2009-2402.

[42] The Scipy community, “scipy.integrate.ode,” *SciPy v0.18.0 Reference Guide*. [Online]. Available: http://docs.scipy.org/doc/scipy/reference/generated/scipy.integrate.ode.html#scipy.integrate.ode. [Accessed: 08-Aug-2016].

[43] Voß, A., “Gust Loads Calculation for a Flying Wing Configuration,” presented at the AIAA AVIATION Forum, Atlanta, Georgia, 2018, https://doi.org/10.2514/6.2018-3326.

[44] Voß, A., and Klimmek, T., “Design and sizing of a parametric structural model for a UCAV configuration for loads and aeroelastic analysis,” *CEAS Aeronautical Journal*, vol. 8, no. 1, pp. 67–77, Mar. 2017, https://doi.org/10.1007/s13272-016-0223-2.

[45] Voß, A., and Klimmek, T., “Maneuver Loads Calculation with Enhanced Aerodynamics for a UCAV Configuration,” in *AIAA AVIATION Forum*, Washington, D.C., 2016, https://doi.org/10.2514/6.2016-3838.

[46] Wang, Lui, Chen, and Mook, “Tightly-Coupled Nonlinear Aerodynamics/Nonlinear Structure Interaction: A HALE Wing Aeroelastic Case Studied,” presented at the International Forum for Aeroelasticity and Structural Dynamics, Stockholm, Sweden, 2007.

[47] Waszak, M., Buttrill, C., and Schmidt, D., “Modeling and Model Simplification of Aeroelastic Vehicles: An Overview,” NASA Langley Research Center, NASA Technical Memorandum 107691, Sep. 1992.

[48] Waszak, M. R., and Schmidt, D. K., “Flight dynamics of aeroelastic vehicles,” *Journal of Aircraft*, vol. 25, no. 6, pp. 563–571, Jun. 1988, https://doi.org/10.2514/3.45623.